ArxiV, astro-ph, 1-11 dec 2015

От О.К. Сильченко

Astro-ph: 1512.00017

LUMINOSITY DEPENDENCE AND REDSHIFT EVOLUTION OF STRONG EMISSION-LINE DIAGNOSTICS IN STAR-FORMING GALAXIES[1]

L. L. Cowie,[2] A. J. Barger,[2,3,4] A. Songaila[2]

To be published in The Astrophysical Journal

ABSTRACT

We examine the redshift evolution of standard strong emission-line diagnostics for Hβ-selected star-forming galaxies using the local SDSS sample and a new $z = 0.2 - 2.3$ sample obtained from *HST* WFC3 grism and Keck DEIMOS and MOSFIRE data. We use the SDSS galaxies to show that there is a systematic dependence of the strong emission-line properties on Balmer-line luminosity, which we interpret as showing that both the N/O abundance and the ionization parameter increase with increasing line luminosity. Allowing for the luminosity dependence tightens the diagnostic diagrams and the metallicity calibrations. The combined SDSS and high-redshift samples show that there is no redshift evolution in the line properties once the luminosity correction is applied, i.e., all galaxies with a given $L(\mathrm{H}\beta)$ have similar strong emission-line distributions at all the observed redshifts. We argue that the best metal diagnostic for the high-redshift galaxies may be a luminosity-adjusted version of the [NII]6584/Hα metallicity relation.

Subject headings: cosmology: observations — galaxies: distances and redshifts — galaxies: active — X-rays: galaxies — galaxies: formation — galaxies: evolution

Эмпирическое приведение к одной светимости в H-beta

Motivated by Figure 5(a), we fitted the dependence of O3Hb on N2Ha and $L(\mathrm{H}\beta)$ for the star-forming galaxy locus (N2Ha < -0.5) using the MPFIT2DFUN two-dimensional fitting routine from Markwardt (2009). We adopted a third-order fit for the dependence on N2Ha and a linear fit for the dependence on $\log L(\mathrm{H}\beta)$. Including the luminosity dependence by shifting N2Ha, we find

$$x = \mathrm{N2Ha} - 0.09(\log L(\mathrm{H}\beta) - 40.5)\,, \qquad (1)$$

and

$$\mathrm{O3Hb} = -1.85 - 4.02x - 2.18x^2 - 0.42x^3\,. \qquad (2)$$

Alternatively, we can include the luminosity dependence by shifting O3Hb, giving

$$\mathrm{O3Hb} = -1.85 - 4.02(\mathrm{N2Ha}) - 2.18(\mathrm{N2Ha})^2 - 0.42(\mathrm{N2Ha})^3 + 0.09(\log L(\mathrm{H}\beta) - 40.5)\,. \qquad (3)$$

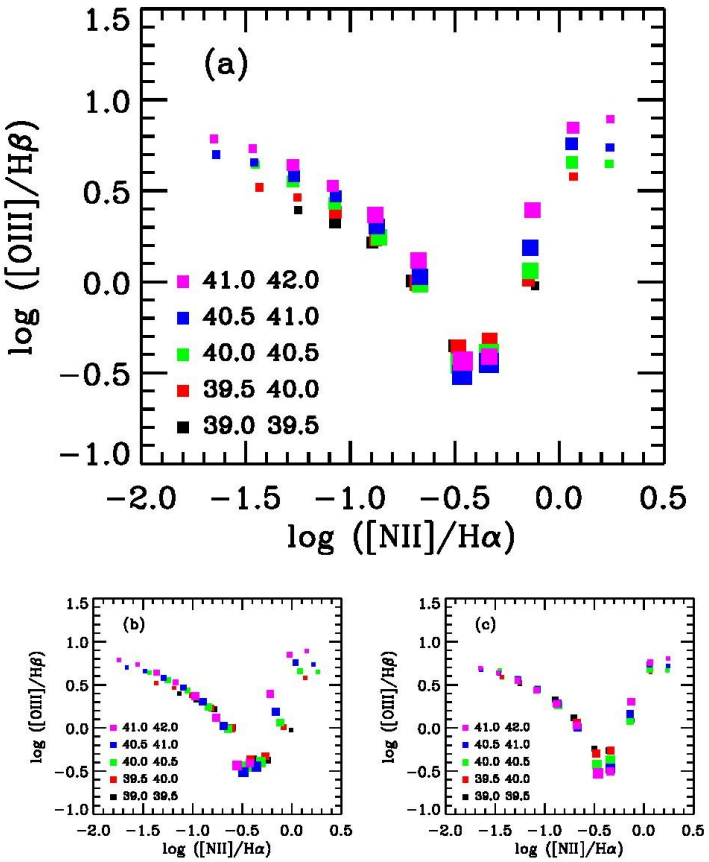

FIG. 5.— (a) BPT diagram for the full SDSS sample in intervals of $\log L(\mathrm{H}\beta)$ (colors). We show the median values of O3Hb in 0.2 dex bins of N2Ha (squares). The sizes of the squares represent the number of sources in each bin, ranging from $10-100$ (smallest), $100-1000$, $1000-10000$, to $10000-100000$ (largest). In the star-forming galaxy locus (the left wing of the BPT diagram; N2Ha < -0.5), the normalization of O3Hb relative to N2Ha rises with $L(\mathrm{H}\beta)$. In (b) and (c), respectively, we show the effects of introducing an offset in N2Ha using Equations 1 and 2 and in O3Hb using Equation 3 to normalize to $\log L(\mathrm{H}\beta) = 40.5$ erg s^{-1}. Either offset approximately aligns the BPT star-forming galaxy locus.

Лучшая калибровка металличности – по азоту, после сдвига

$$12 + \log(\mathrm{O/H}) = 8.90 + 0.57(\mathrm{N2Ha}) - 0.14(\log L(\mathrm{H}\beta) - 41)\,. \quad (10)$$

Эмпирика

$$12 + \log(\mathrm{O/H}) = 9.35 + 0.82\log(\mathrm{N2Ha}) + 0.14(\log L(\mathrm{H}\beta) - 41)\,. \quad (13)$$

Теория (Допита-Кьюли)

Окончательная рекомендация:

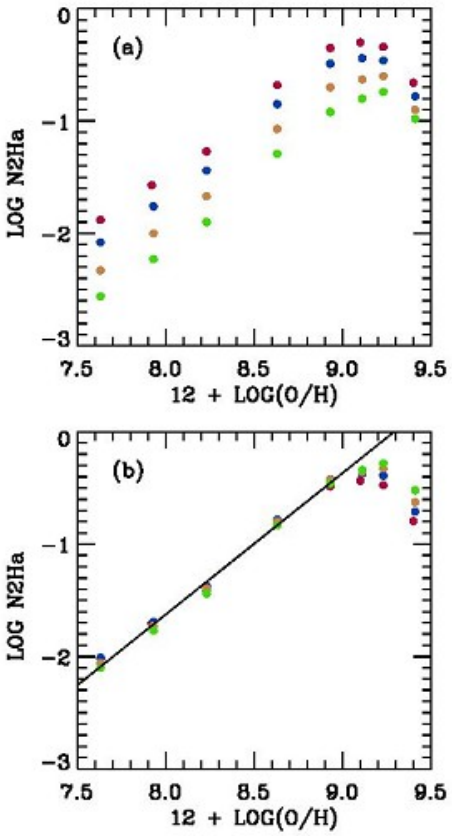

FIG. 14.— N2Ha vs. 12+log(O/H) as a function of the ionization parameter, q. (a) Model calculations of Kewley & Dopita (2002) taken from their Figure 7. The color of the symbols shows the $\log q$ parameter ranging from 8.18 (green), 7.90 (gold), 7.60 (blue), to 7.30 (red). (b) Same points from (a) after applying a correction of $-0.66(\log q - 7.5)$ to NH2a. This brings the points into approximate agreement throughout much of the $12 + \log(O/H)$ range. Below $12+\log(O/H)=9$, the points in (a) are well fit by the linear relation of Equation 12, which is shown for $\log q = 7.5$ as the black line in (b).

- Теория Допита-Кьюли: если нормировать к одной светимости в H-beta, то исчезает зависимость калибровки металличность-отношение от параметра возбуждения

Astro-ph: 1512.00246

Deep MUSE observations in the HDFS ⋆

Morpho-kinematics of distant star-forming galaxies down to 10^8 $M_\odot$

T. Contini[1,2], B. Epinat[1,2,3], N. Bouché[4], J. Brinchmann[5], L. A. Boogaard[5], E. Ventou[1,2], R. Bacon[6], J. Richard[6], P. M. Weilbacher[7], L. Wisotzki[7], D. Krajnović[7], J-B. Vielfaure[1,2], E. Emsellem[8,6], H. Finley[1,2], H. Inami[6], J. Schaye[5], M. Swinbank[9], A. Guérou[8,1,2], T. Martinsson[5,10,11], L. Michel-Dansac[6], I. Schroetter[1,2], M. Shirazi[12], and G. Soucail[1,2]

[1] IRAP, Institut de Recherche en Astrophysique et Planétologie, CNRS, 14, avenue Edouard Belin, F-31400 Toulouse, France
[2] Université de Toulouse, UPS-OMP, Toulouse, France
[3] Aix Marseille Université, CNRS, LAM, Laboratoire d'Astrophysique de Marseille, UMR 7326, 13388, Marseille, France
[4] IRAP/CNRS, 9, avenue Colonel Roche, F-31400 Toulouse, France
[5] Leiden Observatory, Leiden University, P.O. Box 9513, 2300 RA Leiden, The Netherlands
[6] CRAL, Observatoire de Lyon, CNRS, Université Lyon 1, 9 Avenue Ch. André, F-69561 Saint Genis Laval Cedex, France
[7] Leibniz-Institut für Astrophysik Potsdam (AIP), An der Sternwarte 16, D-14482 Potsdam, Germany
[8] ESO, European Southern Observatory, Karl-Schwarzschild Str. 2, 85748 Garching bei Muenchen, Germany
[9] Institute for Computational Cosmology, Durham University, South Road, Durham DH1 3LE, UK
[10] Instituto de Astrofisica de Canarias (IAC), E-38205 La Laguna, Tenerife, Spain
[11] Departamento de Astrofisica, Universidad de La Laguna, E-38206 La Laguna, Tenerife, Spain
[12] ETH Zurich, Institute of Astronomy, Wolfgang-Pauli-Str. 27, CH-8093 Zurich, Switzerland

Поле HDFS

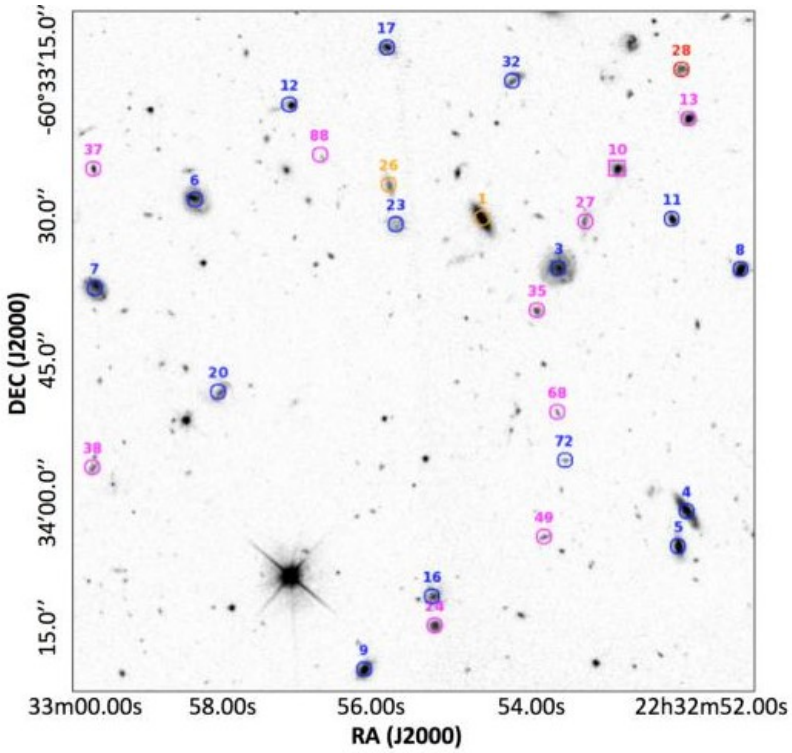

Fig. 1. Location of the spatially-resolved galaxies selected in the MUSE-HDFS data cube overlaid on the HST/WFPC2 F814W image. The diameter of the circles is equal to the effective spatial resolution ($\approx 0.7''$ FWHM) of the MUSE data cube. Identification numbers are those from the source catalogue of Bacon et al. (2015). The AGN ID#10 is indicated with a square. Colors correspond to different redshift intervals and thus to different set of bright emission lines accessible within the spectral range of MUSE (orange = $z < 0.27$: from Hβ

Результат MUSE

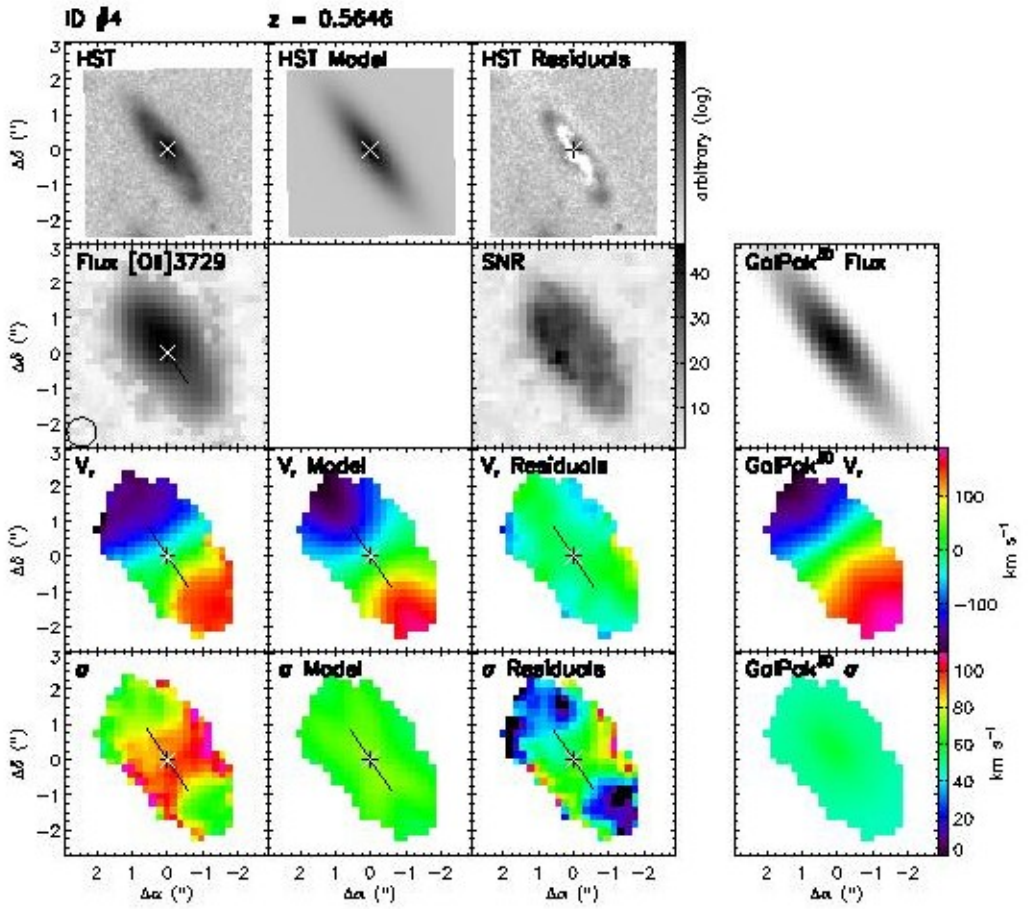

Fig. 5. Example of morpho-kinematic analysis for galaxy ID#4 at $z \approx 0.56$. Description is given from *left* to *right*. *Top* row: HST/WFPC2

Результат анализа

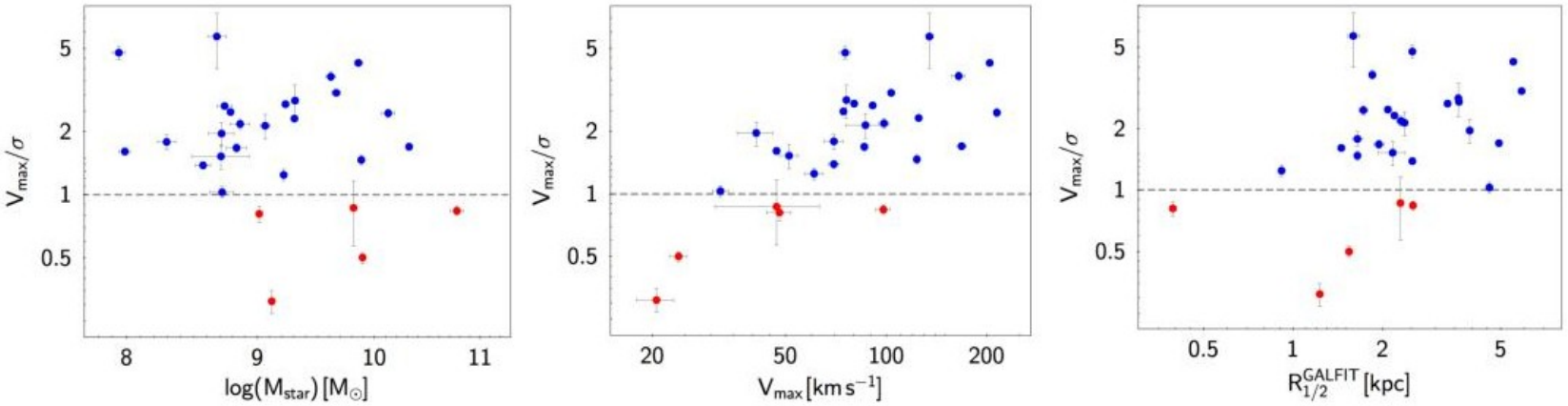

Fig. 8. The ratio V/σ as a function of galaxy stellar mass (*left panel*), maximum rotational velocity (*middle panel*) and size (*right panel*). The horizontal dashed lines set the limit between rotation-dominated (blue points above the line) and dispersion-dominated (red points below the line) galaxies. No clear correlation is seen but dispersion-dominated galaxies are mostly massive ($> 10^9 M_\odot$), "slow" rotators (≤ 50 km s^{-1}) and quite compact.

Заяв

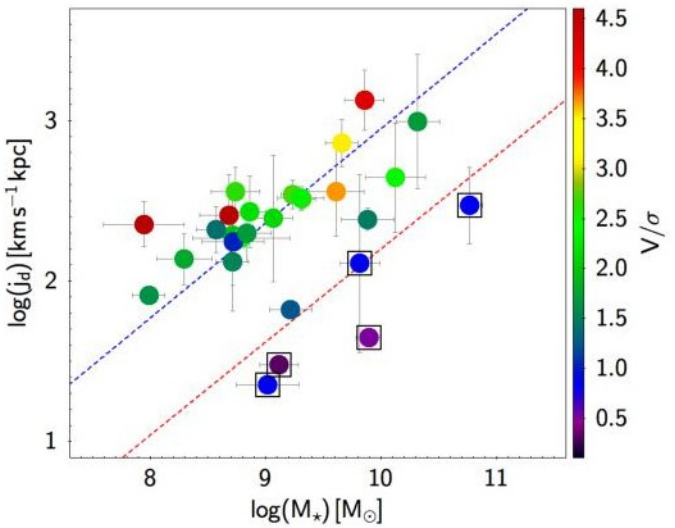

Fig. 12. The specific angular momentum of disks j_d as a function of galaxy stellar mass for the MUSE-HDFS sample of spatially-resolved galaxies. Data points are color-coded according to the V/σ ratio. Large squares indicate dispersion-dominated galaxies with $V/\sigma < 1$. The dashed lines show the relations defined for massive ($M_\star > 10^{10}$ $M_\odot$) galaxies at $z = 0$ (Fall & Romanowsky 2013), distinguishing between spheroids (red line) and disks (blue line).

Astro-ph: 1512.00477

Possible Population III Remnants at Redshift 3.5

Neil H. M. Crighton,[1]★ John M. O'Meara[2] and Michael T. Murphy[1]
[1]*Centre for Astrophysics and Supercomputing, Swinburne University of Technology, Hawthorn, Victoria 3122, Australia*
[2]*Department of Chemistry & Physics, Saint Michael's College, One Winooski Park, Colchester VT, 05439*

To appear in MNRAS letters

ABSTRACT

The first stars, known as Population III (PopIII), produced the first heavy elements, thereby enriching their surrounding pristine gas. Previous detections of metals in intergalactic gas clouds, however, find a heavy element enrichment larger than 1/1000 times that of the solar environment, higher than expected for PopIII remnants. In this letter we report the discovery of a Lyman limit system (LLS) at $z = 3.53$ with the lowest metallicity seen in gas with discernable metals, $10^{-3.41\pm0.26}$ times the solar value, at a level expected for PopIII remnants. We make the first relative abundance measurement in such low metallicity gas: the carbon-to-silicon ratio is $10^{-0.26\pm0.17}$ times the solar value. This is consistent with models of gas enrichment by a PopIII star formation event early in the Universe, but also consistent with later, Population II enrichment. The metals in all three components comprising the LLS, which has a velocity width of 400 km s^{-1}, are offset in velocity by $\sim +6$ km s^{-1} from the bulk of

Линии далекой галактики на просвет

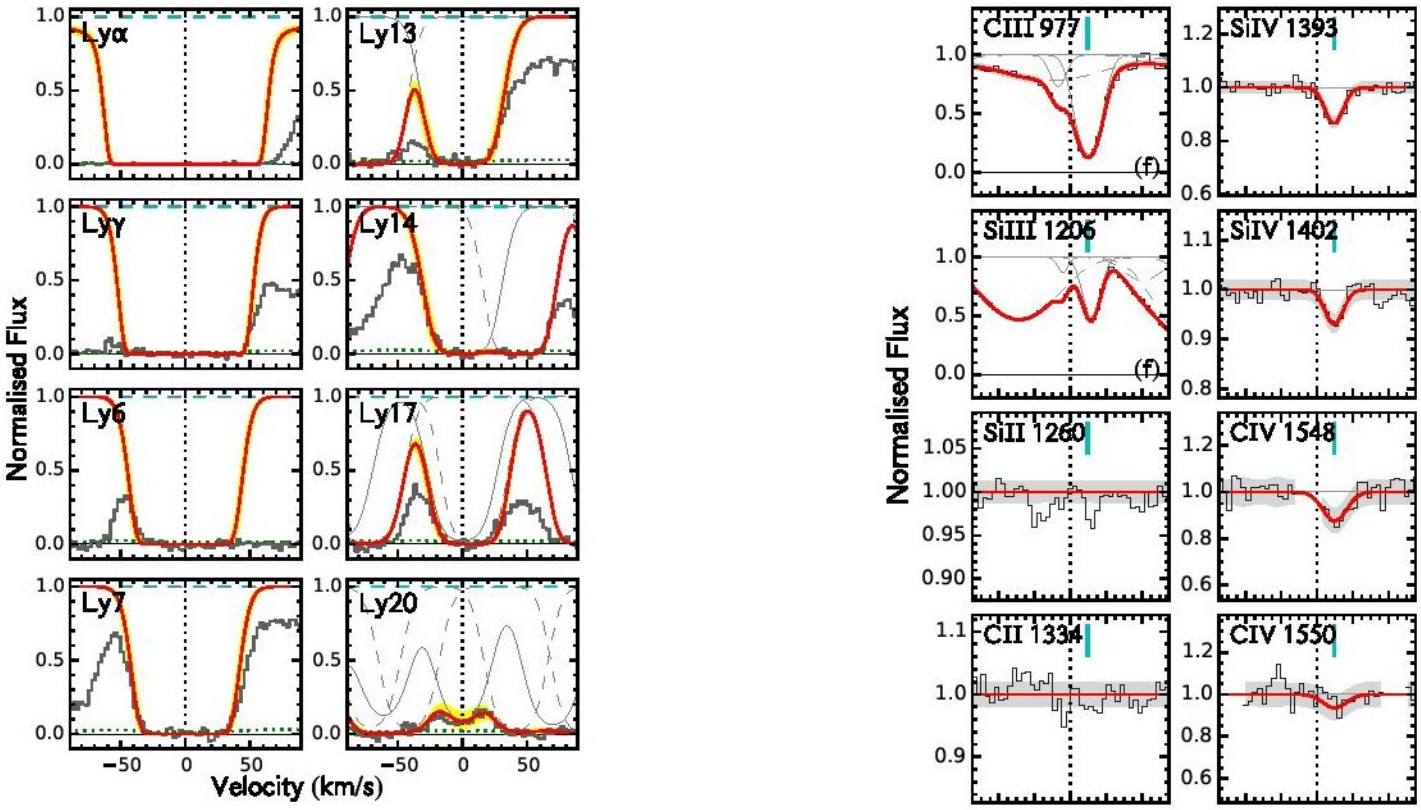

Эпохальный результат

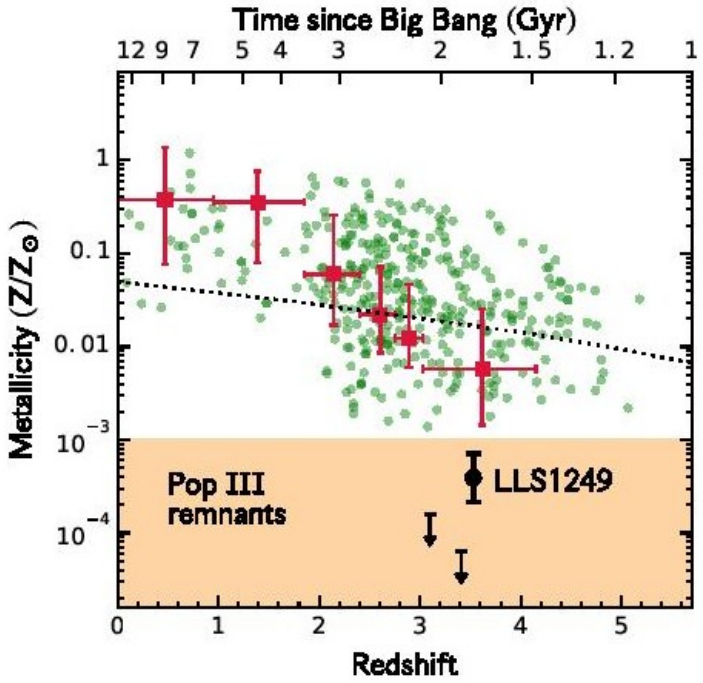

Figure 5. The metallicity of LLS1249 compared to other measurements of diffuse gas metallicities. Green dots show representative metallicities for the predominantly neutral damped Lyman-α systems (see text); their typical uncertainties are 0.2 dex. Red squares show metallicities for a compilation of the more highly ionized Lyman limit systems (Fumagalli et al. 2015). Vertical errors on the squares show the 25–75% range in the sample metallicity probability distribution. Upper limits from Fumagalli et al.

Astro-ph:1512.02342

Galaxy And Mass Assembly (GAMA): the Stellar Mass Budget by Galaxy Type

Amanda J. Moffett,[1†] Stephen A. Ingarfield,[1] Simon P. Driver,[1,3] Aaron S. G. Robotham,[1] Lee S. Kelvin,[2,5] Rebecca Lange,[1] Uroš Meštrić,[2] Mehmet Alpaslan,[4] Ivan K. Baldry,[5] Joss Bland-Hawthorn,[6] Sarah Brough,[7] Michelle E. Cluver,[8] Luke J. M. Davies,[1] Benne W. Holwerda,[9] Andrew M. Hopkins,[7] Prajwal R. Kafle,[1] Rebecca Kennedy,[10] Peder Norberg,[11] and Edward N. Taylor[12]

[1] *ICRAR, The University of Western Australia, 35 Stirling Highway, Crawley WA 6009, Australia*
[2] *Institute für Astro- und Teilchenphysik, Universität Innsbruck, Technikerstraße 25, 6020 Innsbruck, Austria*
[3] *SUPA, School of Physics & Astronomy, University of St Andrews, North Haugh, St Andrews, KY16 9SS, UK*
[4] *NASA Ames Research Center, N232, Moffett Field, Mountain View, CA 94035, United States*
[5] *Astrophysics Research Institute, Liverpool John Moores University, IC2, Liverpool Science Park, 146 Brownlow Hill, Liverpool, L3 5RF*
[6] *Sydney Institute for Astronomy, School of Physics A28, University of Sydney, NSW 2006, Australia*
[7] *Australian Astronomical Observatory, PO Box 915, North Ryde, NSW 1670, Australia*
[8] *Department of Physics, University of the Western Cape, Robert Sobukwe Road, Bellville, 7535, South Africa*
[9] *Leiden Observatory, University of Leiden, Niels Bohrweg 2, 2333 CA Leiden, The Netherlands*
[10] *School of Physics & Astronomy, The University of Nottingham, University Park, Nottingham, NG7 2RD, UK*
[11] *ICC & CEA, Department of Physics, Durham University, Durham DH1 3LE, UK*
[12] *School of Physics, the University of Melbourne, VIC 3010, Australia*
[†] *E-mail: amanda.moffett@uwa.edu.au*

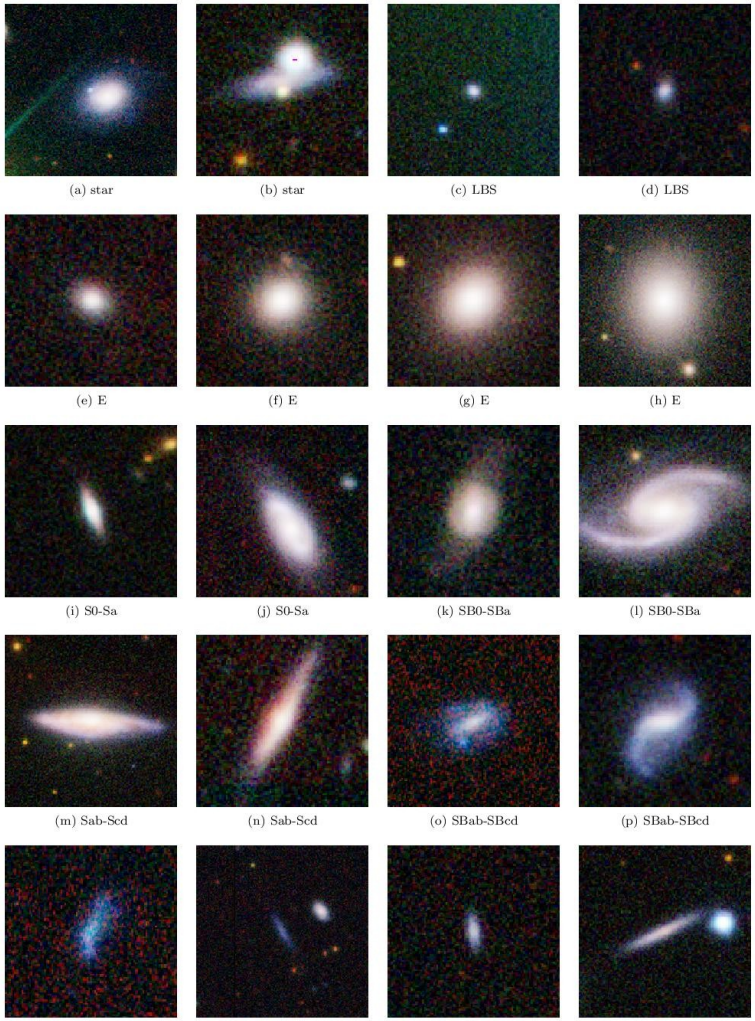

(a) star (b) star (c) LBS (d) LBS

(e) E (f) E (g) E (h) E

(i) S0-Sa (j) S0-Sa (k) SB0-SBa (l) SB0-SBa

(m) Sab-Scd (n) Sab-Scd (o) SBab-SBcd (p) SBab-SBcd

(q) Sd-Irr (r) Sd-Irr (s) Sd-Irr (t) Sd-Irr

Figure 2. Example three-colour (giH) classification images covering a physical distance of 30kpc on a side, as described in §3.1. Each image is labelled with its assigned type according to the hierarchy illustrated in Fig. 3.

Морфологические классы

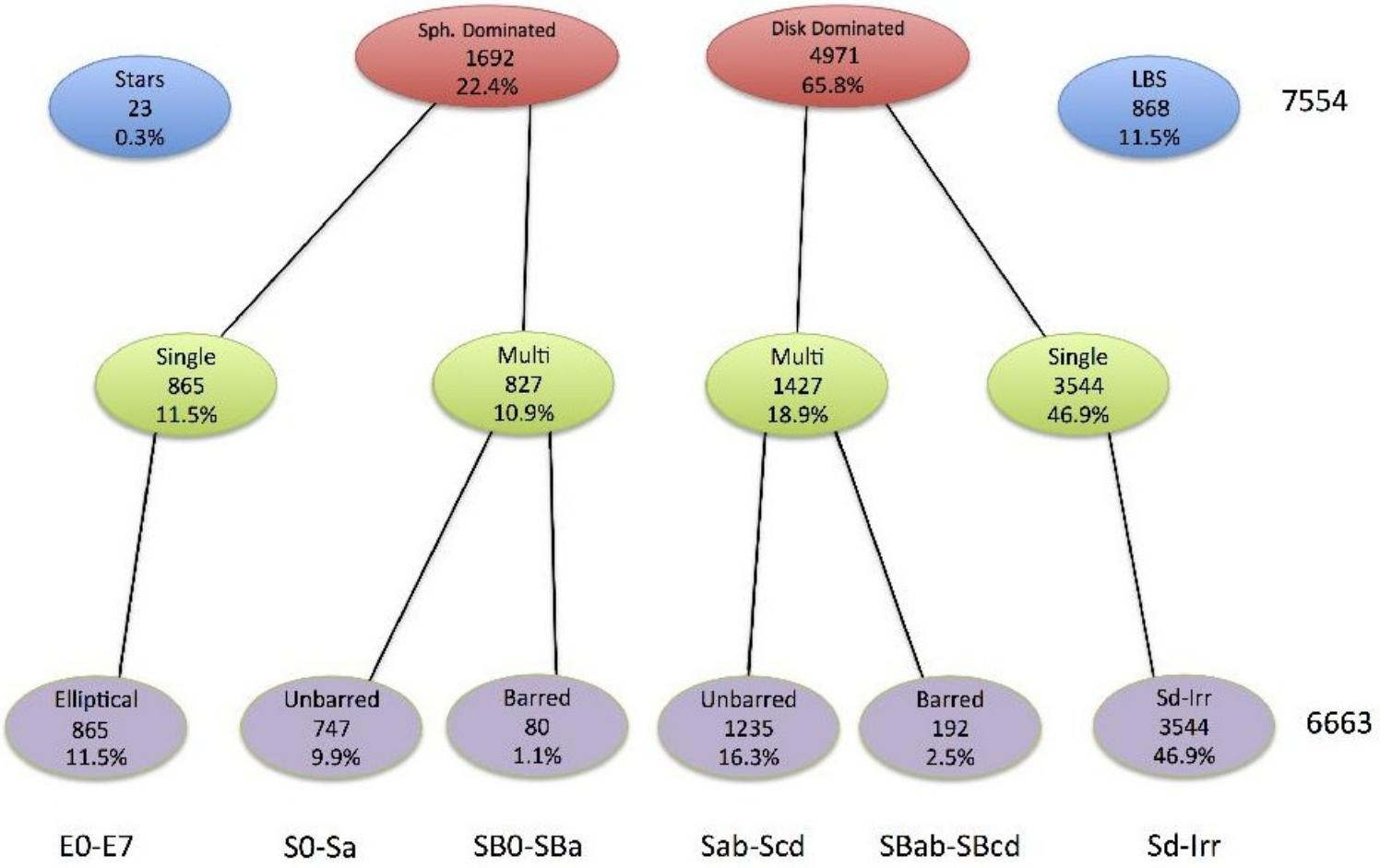

Figure 3. Morphological classification hierarchy used to filter the GAMA-II sample of 7,554 galaxies into their appropriate class.

Массы

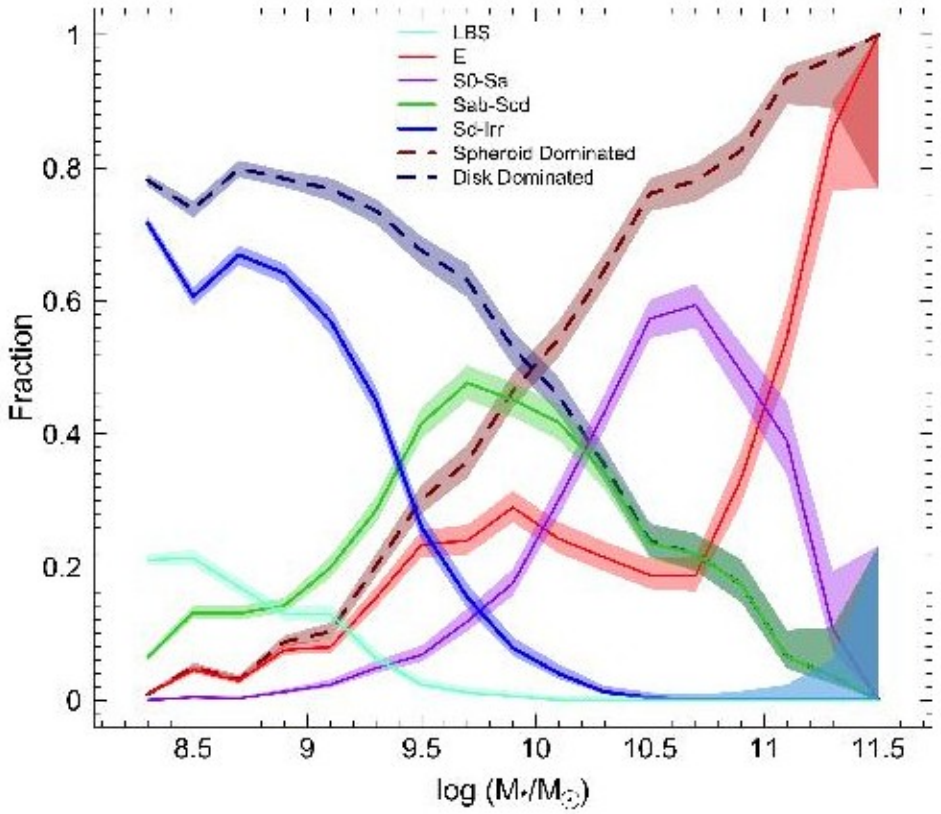

Figure 5. Fractional contribution of various morphological types to the total by number as a function of stellar mass, with $V/V_{\max}$ weights applied. Spheroid-dominated and disk-dominated classes

Результаты Пресс-Шехтер приближения функций масс по типам

Table 1. Single Schechter stellar mass function fit parameters for the morphological-type stellar mass functions in Figs. 6 and 8. Columns are: the knee in the Schechter function (M^*), the slope (α), and the normalization constant (ϕ^*). Quoted error bars are derived from the spread in each parameter's posterior probability distribution from fits carried out in 10 jackknife resampling iterations.

Population	$\log(M^* h_{0.7}{}^2/M_\odot)$	α	$\phi^*/10^{-3}$ $(\mathrm{dex}^{-1}\mathrm{Mpc}^{-3}h_{0.7}{}^3)$
E	11.02 ± 0.055	-0.888 ± 0.034	$0.865^{+1.0}_{-0.63}$
S0-Sa	10.44 ± 0.028	0.127 ± 0.064	$2.90^{+0.15}_{-0.16}$
Sab-Scd	10.39 ± 0.034	-0.734 ± 0.033	$2.43^{+0.14}_{-0.14}$
Sd-Irr	9.755 ± 0.062	-1.69 ± 0.054	$1.14^{+0.27}_{-0.22}$
LBS	9.300 ± 0.12	-1.71 ± 0.15	$0.738^{+0.43}_{-0.28}$
Spheroid Dominated	10.74 ± 0.026	-0.525 ± 0.029	$3.67^{+0.20}_{-0.20}$
Disk Dominated	10.70 ± 0.049	-1.39 ± 0.021	$0.855^{+0.10}_{-0.093}$

Table 2. Total stellar mass densities and stellar mass densities for each morphological class, derived both by summation of data with V/V_{max} weights (ρ_Σ) and integration of stellar mass functions (ρ_ϕ). A fraction of the total stellar mass is also given for each subclass and method. Quoted error bars are derived according to a jackknife resampling procedure as decribed in §4.2. Derived stellar mass density estimates should also be subject to an additional 22.3% error contribution from cosmic variance, estimated by the method of Driver & Robotham (2010).

Population	$\rho_\Sigma/10^7$ $(M_\odot\mathrm{Mpc}^{-3}h_{0.7})$	Fraction of All (sum)	$\rho_\phi/10^7$ $(M_\odot\mathrm{Mpc}^{-3}h_{0.7})$	Fraction of All (fit)
All	24 ± 7.9	...	25 ± 5.6	...
E	8.3 ± 2.9	0.34	8.7 ± 4.3	0.35
S0-Sa	9.2 ± 3.0	0.38	8.6 ± 1.2	0.34
Sab-Scd	5.1 ± 1.6	0.21	5.4 ± 0.63	0.22
Sd-Irr	1.3 ± 0.40	0.052	1.9 ± 0.29	0.074
LBS	0.23 ± 0.069	0.0094	0.45 ± 0.22	0.018
Spheroid Dominated	17 ± 5.9	0.73	18 ± 3.2	0.71
Disk Dominated	6.3 ± 2.0	0.26	6.2 ± 0.82	0.25

Astro-ph: 1512.01558

Submitted to Nature, embargoed for discussion in the press until further notice

Copious r-process enrichment from a single event in an ancient dwarf galaxy

Alexander P. Ji[*], Anna Frebel[*†], Anirudh Chiti[*], Joshua D. Simon[‡]

The elements heavier than zinc are synthesized through the (r)apid and (s)low neutron-capture processes[1,2]. The primary astrophysical production site of the r-process elements (such as europium) has been debated for nearly 60 years[2]. Chemical abundance trends of old Galactic halo stars initially suggested continual r-process production from sources like core-collapse supernovae[3,4], but evidence in the local universe favored r-process production primarily from rare events like neutron star mergers[5,6]. The appearance of a europium abundance plateau in some dwarf spheroidal galaxies was suggested as evidence for rare r-process enrichment in the early universe[7], but only under the assumption of no gas accretion into the dwarfs. Invoking cosmologically motivated gas accretion[8] actually favors continual r-process enrichment in those systems. Furthermore, the universal r-process pattern[1,9] has not been cleanly identified in those galaxies. The smaller, chemically simpler, and more ancient ultra-faint dwarf galaxies (UFDs) assembled shortly after the formation of the first stars and are ideal systems to study nucleosynthesis processes such as the r-process[10,11]. Here we report that seven of nine stars observed with high-resolution spectroscopy in the recently discovered UFD Reticulum II[12,13] show strong enhancements in heavy neutron-capture elements with abundances that exactly follow the universal r-

Результаты для Reticulum II в сравнении с…

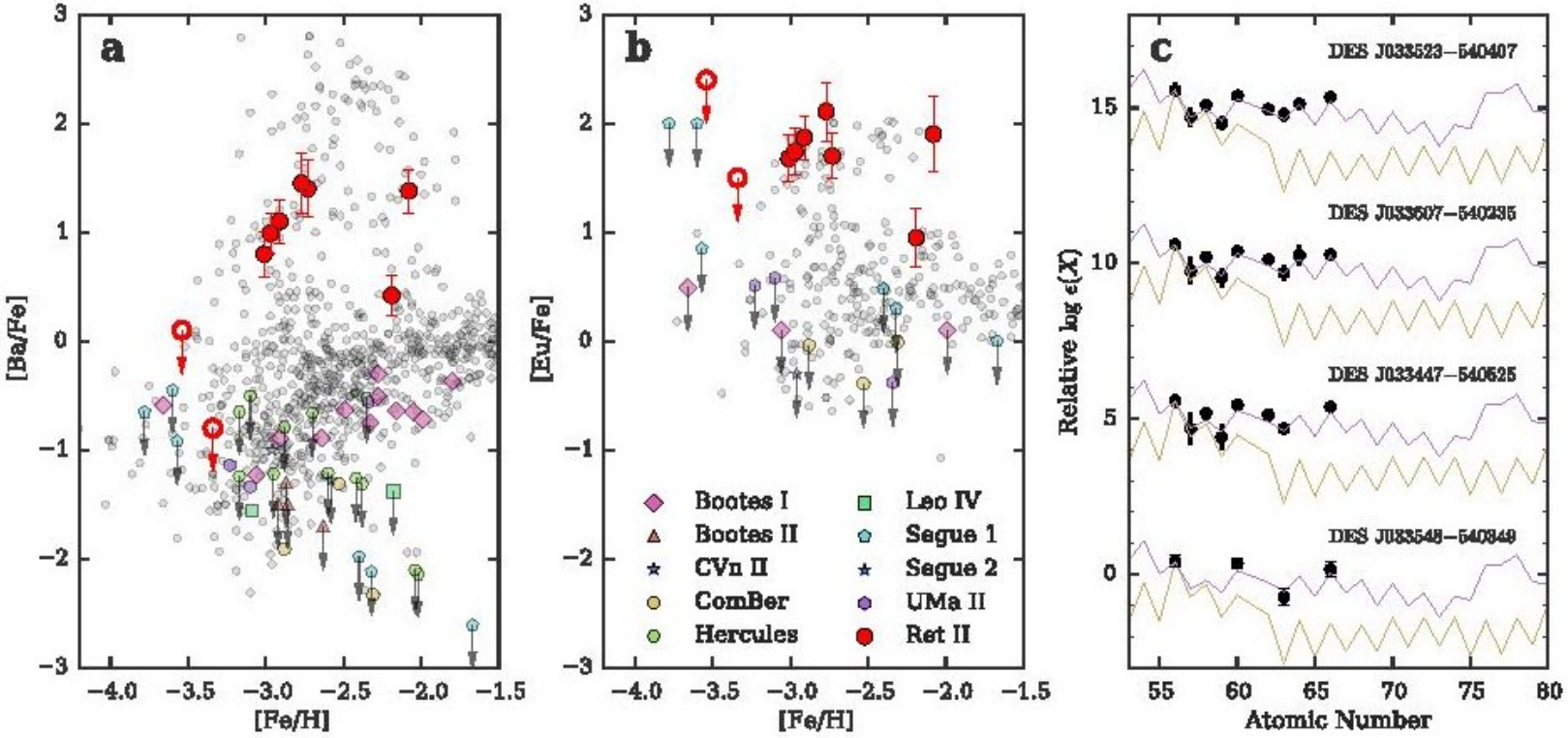

Figure 2: Chemical abundances of stars in Reticulum II.
Panels a-b: Abundances of neutron-capture elements Ba and Eu for stars in Ret II (large red points) compared to halo stars[23] (small gray points) and UFD stars in Segue 1, Hercules, Leo IV, Segue 2, Canes Venatici II, Bootes I, Bootes II, Ursa Major II, and Coma Berenices (medium colored points, see references in refs. [11,14,15]). Arrows denote upper limits. The notation